A neutron diffraction and Rietveld analysis of cooperative Li motion in beta-eucryptite

2004 J. Phys.: Condens. Matter 16 5267

(http://iopscience.iop.org/0953-8984/16/29/018)

INSTITUTE OF PHYSICS PUBLISHING JOURNAL OF PHYSICS: CONDENSED MATTER

J. Phys.: Condens. Matter **16** (2004) 5267–5278 PII: S0953-8984(04)78518-5

A neutron diffraction and Rietveld analysis of cooperative Li motion in beta-eucryptite

Asel Sartbaeva[1], Simon A T Redfern[1] and William T Lee[1,2]

[1] Department of Earth Sciences, University of Cambridge, Downing Street, Cambridge CB2 3EQ, UK
[2] Mineralogisch-Petrographisches Institut, Universität Hamburg, Grindelallee 48, 20146 Hamburg, Germany

E-mail: asar01@esc.cam.ac.uk

Received 29 March 2004
Published 9 July 2004
Online at stacks.iop.org/JPhysCM/16/5267
doi:10.1088/0953-8984/16/29/018

Abstract

Li^+ mobility and structural changes in the aluminosilicate beta-eucryptite have been studied by high-resolution powder neutron diffraction as a function of temperature from 573 to 873 K. A Li split-atom model was used to describe the disorder of Li^+ ions in the structure. Analysis of the data shows two anomalies around 698 and 758 K. The first anomaly is attributed to an M-point zone boundary transition reported in the literature, which is connected to the appearance of the incommensurate structure. The second anomaly is attributed to a displacive phase transition of the framework and doubling in the *a* cell parameter.

1. Introduction

Beta-eucryptite ($LiAlSiO_4$) is known as a stuffed derivative of the quartz structure [1]. There are four distinct tetrahedral sites in the structure: T_1–T_4. The structure consists of alternating layers of T_1 and T_2, and T_3 and T_4 tetrahedra. In the ordered form, Si occupies T_1 and T_2 sites, and Al occupies T_3 and T_4 sites (figure 1). Thus, half of the silicon atoms are replaced by aluminium, with silicon and aluminium tetrahedra stacked alternately along the *c*-axis. Charge is balanced by the incorporation of lithium ions in the channels of the structure, which run parallel to the *c*-axis. The unit cell contains one primary and three secondary channels. In each unit cell there are six possible sites for the lithium ions, fourfold coordinated by oxygen, only three of which are occupied on average in the ideal structure.

Beta-eucryptite has been a subject of continuing interest because of its one-dimensional superionic conductivity, due to lithium ion transport in the structural channels [2]. It also exhibits near-zero overall thermal expansion [3–5]. The symmetry and extinction of the main

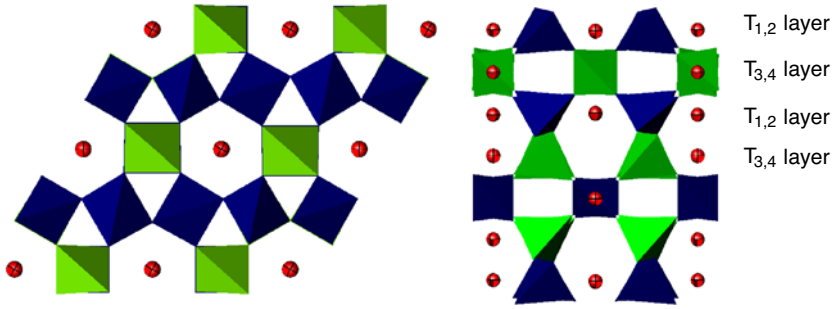

Figure 1. Structure of ordered beta-eucryptite, (a) projected down [001]; (b) projected onto (100). Dark blue tetrahedra are $T_{1,2}$ sites (Si), light green tetrahedra are $T_{3,4}$ sites (Al), oxygen atoms are in the corners of the tetrahedra and red are Li atoms inside the channels.

(This figure is in colour only in the electronic version)

reflections in single crystal x-ray diffraction patterns indicates that at ambient temperatures beta-eucryptite has the high-quartz space group $P6_422$ or $P6_222$, although the unit cell is doubled ($2 \times 2 \times 2$) [6, 7].

The crystal structure of beta-eucryptite has been studied by Pillar and Peacor as a function of temperature [8], using a single-crystal diffractometer at six temperatures, in the temperature range from 296 to 920 K. It was suggested that there is a second-order phase transition in beta-eucryptite at 733 K, and that Li order–disorder is the primary driving factor for the transition. Above this temperature the superstructure reflections, arising in part from distortions of the quartz-structure-type framework, decrease in intensity and become unobservable. Press *et al* (1980) studied beta-eucryptite by slow neutron single-crystal diffraction from 293 to 823 K [9]. In the temperature range from 703 to 763 K, Press *et al* found an incommensurate structure which coexists with the low-temperature superstructure between 703 and 755.5 K. The phase transition at 763 K not only involves an ordering of lithium along chains, but also is accompanied by a distortion of the Al/Si framework. Thus it partly has the character of a displacive transition, while the lithium ordering rather has the character of an order–disorder transition of Li ion positions. In 1981, Nara *et al* [10] proposed a theory for the commensurate–incommensurate phase transition, based on neutron scattering data. Nara also suggested that the transition at 755.5 K only shows a small discontinuity and thus is close to second order. In 1999, Xu *et al* [7] reported on the study of Press [9]: in addition to the phase transitions described before, one more transition at 723 K was proposed. Xu *et al* argued that all the phase transitions in beta-eucryptite are due to the positional disordering of the lithium ions along the structural channels, without distortion in the Si/Al framework. In addition, Xu *et al* [11] investigated thermal expansion in ordered and disordered β-eucryptite by combined synchrotron x-ray and neutron Rietveld analysis. The near-zero thermal expansion was attributed to three processes: Al/Si tetrahedral deformation, Li positional disordering and tetrahedral tilting. Different degrees of Li positional disorder was found in both ordered and disordered samples, and modelling the Li ion motion in the channels has proved to be very difficult. Many authors agree that a thermal ellipsoid about the average site does not describe the Li ion dynamic disorder correctly [7, 12]. Most recently, in an infrared study, Zhang *et al* [13] proposed that there are two phase transitions around 715 and 780 K in beta-eucryptite. The first phase transition was attributed to the Li^+ disorder.

The aim of the present work was to study Li ion mobility and the structure of beta-eucryptite by high-resolution neutron diffraction, hence data were obtained from 573 up to

873 K. Since the reported temperatures for the phase transitions were not consistent, we were also interested in obtaining information about the temperatures and thermodynamic character of the phase transitions.

2. Experimental details

2.1. Sample synthesis

Beta-eucryptite was synthesized from Li_2CO_3 (Aldrich 99.999%), Al_2O_3 (Aldrich 99.99%) and $SiO_2{\cdot}H_2O$ (Aldrich 99.99%) powders in the molar ratio 1:1:2. The mixture was sintered at 1373 K for 15 h and, after grinding, resintered at 1573 K for 24 h and at 1373 K for another 24 h. X-ray powder diffraction analysis showed that the final material consisted of pure beta-eucryptite.

2.2. Neutron data collection and Rietveld refinement

Neutron diffraction experiments were performed at the D2B powder diffractometer at the ILL, Grenoble. We collected data at 573, 623, 663, 683, 703, 733, 743, 753, 763, 773, 793, 823 and 873 K. The wavelength used was 1.549 Å. Data were collected from 5° to 165° 2θ. The sample was sealed in a 16 mm diameter vanadium can. The sample temperature was determined using two thermocouples, positioned on either side of the sample. The structure was refined by the Rietveld method using the general structure analysis system (GSAS) program of Larson and Von Dreele [14]. The starting model for the refinement was modified from the model of Xu *et al* [11]. All the Li coordinates were moved slightly from the ideal starting points. This resulted in quartets and pairs of each atom around the idealized site, allowing us to model positional disorder of the Li ions. The occupancies were constrained in order to obtain the stoichiometric amount of Li in the structure. This ensured that we can obtain an idea of relative magnitudes of Li disorder in both the z-direction and in the xy-plane. The temperature factors for Li atoms became very small compared to the starting model, as most of the disorder of atoms was represented by the changes in fractional coordinates of split sites. As for the Si/Al framework, to ensure the right composition several constraints were used. The refinement constrained the occupancy ratio $Si_1 + Al_1' = Si_2 + Al_2' = Al_1 + Si_1' = Al_2 + Si_2' = 1$, and for the fractional coordinates $x(Si_1) = x(Al_1')$, $x(Si_2) = x(Al_2')$, $y(Si_2) = y(Al_2')$, $x(Al_1) = x(Si_1')$, $x(Al_2) = x(Si_2')$, $y(Al_2) = y(Si_2')$. Temperature factors for tetrahedral sites were constrained to be the same.

Our refinement proceeded as follows. Initially we refined the background function with nine variables, and specimen displacement, histogram scale and lattice parameters were optimized. Then profile coefficients were refined. On convergence of these parameters, atomic positions and temperature factors for Si, Al and O were refined. Split-Li positional coordinates were refined last. All parameters were refined to convergence (figure 2). Table 1 presents refined fractional coordinates and temperature factors at 573 K. We then used the refined structural parameters at each temperature as the starting model for the next temperature and continued this procedure systematically with changing temperature. The refined unit cell parameters are listed in table 2, together with R_{wp} and R_p factors.

3. Results and discussion

In our refined structure a number of structural parameters show anomalies at two temperatures: 695 and 758 K. We interpret these anomalies as two phase transitions, one being associated

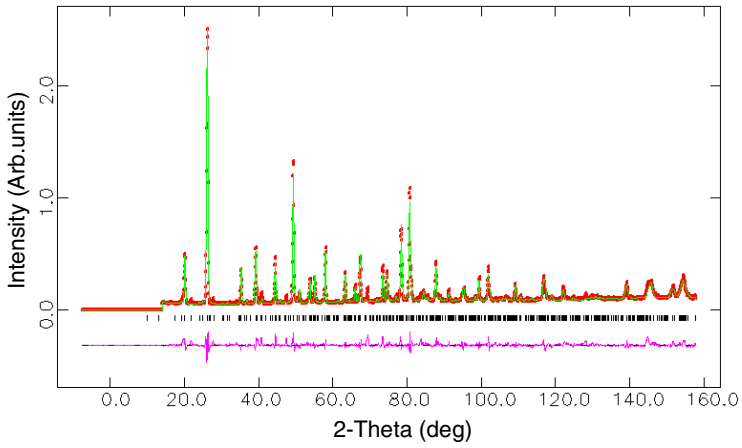

Figure 2. Neutron diffraction pattern of beta-eucryptite at 573 K in 2θ. Dots (red) are data, the upper (green) curve is fit and the lower (purple) curve is the difference.
(This figure is in colour only in the electronic version)

Table 1. Refined fractional coordinates and temperature factors for beta-eucryptite at 573 K with the Li split model. Standard errors are in parentheses.

	x	*y*	*z*	Occupancy	UISO
O_1	0.1015(17)	0.2018(18)	0.2399(7)	1.00	0.0203(25)
O_2	0.0917(11)	0.7011(13)	0.2648(7)	1.00	0.0154(19)
O_3	0.5974(14)	0.6986(13)	0.2626(9)	1.00	0.0193(25)
O_4	0.5994(14)	0.2039(16)	0.2540(8)	1.00	0.0168(19)
Si_1	0.2500(24)	0.0	0.0	0.50	0.0191(13)
Si_2	0.2504(15)	0.5006(20)	0.5	0.50	0.0191(13)
Al_1	0.2528(24)	0.0	0.5	0.50	0.0129(13)
Al_2	0.2482(16)	0.4964(22)	0.5	0.50	0.0129(13)
Al'_1	0.2500(24)	0.0	0.0	0.50	0.0129(13)
Al'_2	0.2504(15)	0.5006(30)	0.5	0.50	0.0129(13)
Si'_1	0.2528(24)	0.0	0.5	0.50	0.0191(13)
Si'_2	0.2482(16)	0.4964(32)	0.5	0.50	0.0191(13)
Li_1	−0.0215(25)	−0.0120(26)	0.5274(15)	0.25	0.0044(18)
Li_2	0.4791(26)	0.0039(33)	0.1784(17)	0.25	0.0044(18)
Li_3	0.4810(26)	−0.0068(28)	0.3078(15)	0.50	0.0044(18)

primarily with Li ion ordering [15] in the structural channels, while the second is a displacive framework transition accompanied by doubling of the *a* cell parameter.

3.1. Framework distortion and transition at 758 K

The refinement with the idealized Si/Al framework (for example the idealized model from [7]) fitted poorly with R_{wp} of 10.24%. As a comparison refinement of our data in the high-temperature space group [16] yields a R_{wp} factor of 11.5%. The best fit was obtained from 50/50 complete disorder in the Si/Al framework, which corresponds to the disorder frozen in from our conditions of synthesis. The analyses of the neutron data show a large distortion of T_1–T_4 tetrahedra compared to [16]. The disordered model is consistent with the calculated $\langle T_{1-4}\text{–O}\rangle$ bond lengths which are intermediate between ideal Si–O and Al–O bond lengths.

Table 2. Unit cell parameters and R-factors as a function of temperature. Standard errors are in parentheses.

Temperature (K)	a (Å)	c (Å)	V (Å^3)	R_p (%)	R_{wp} (%)	χ^2
573	10.522 43(21)	11.107 70(44)	1065.090(41)	5.88	7.53	4.47
623	10.524 83(21)	11.102 10(44)	1064.839(41)	5.92	7.58	4.49
663	10.528 31(21)	11.092 77(44)	1064.849(42)	5.94	7.61	4.51
683	10.530 10(21)	11.089 11(44)	1064.859(43)	5.78	7.43	4.38
703	10.531 89(21)	11.085 35(44)	1064.860(42)	5.75	7.35	4.10
733	10.534 41(21)	11.080 21(44)	1064.876(42)	5.67	7.29	3.85
743	10.535 46(21)	11.078 87(43)	1064.960(42)	5.61	7.16	3.72
753	10.536 17(22)	11.077 51(43)	1064.972(42)	5.58	7.15	3.71
763	10.537 22(22)	11.075 61(43)	1065.003(41)	4.93	6.99	3.56
773	10.538 16(22)	11.073 90(44)	1065.037(42)	5.59	7.18	3.68
793	10.539 67(22)	11.071 57(43)	1065.109(42)	5.57	7.17	3.55
823	10.542 49(22)	11.065 94(44)	1065.136(42)	5.63	7.29	3.55
873	10.546 24(23)	11.058 51(44)	1065.180(42)	5.61	7.13	3.45

Table 3. Selected mean bond lengths, bond angles in Å and degrees and their standard deviations for beta-eucryptite at 573, 743 and 873 K. Standard errors are in parentheses.

	573 (K)	743 (K)	873 (K)
	'Si' tetrahedra		
$\langle T_1–O\rangle$	1.6689(4)	1.6733(4)	1.6852(4)
$\langle T_2–O\rangle$	1.6574(4)	1.6681(4)	1.6615(4)
$\langle O–T_{1,2}–O\rangle$	109.593	109.597	109.599
$\sigma\langle O–T_1–O\rangle$	5.9	9.1	9.2
$\sigma\langle O–T_2–O\rangle$	8.4	5.5	5.2
	'Al' tetrahedra		
$\langle T_3–O\rangle$	1.6605(4)	1.6676(4)	1.6663(4)
$\langle T_4–O\rangle$	1.7056(4)	1.6858(4)	1.6798(4)
$\langle O–T_{3,4}–O\rangle$	109.454	109.414	109.439
$\sigma\langle O–T_3–O\rangle$	5.8	5.3	5.1
$\sigma\langle O–T_4–O\rangle$	5.1	7.7	8.3

This is shown by selected average bond lengths and bond angles for several temperatures, which are listed in table 3. Both $T_{1,2}$–O and $T_{3,4}$–O deviate from 1.606 and 1.757 Å respectively, which are the extrapolated mean values for the framework silicates with completely ordered Si and Al [17]. Our $\langle$T–O$\rangle$ bond distance for $T_{1,2}$ tetrahedra is longer than that calculated from ionic radii and the value extrapolated by Xu *et al* [11], which was 1.63 Å. The $\langle$T–O$\rangle$ bond length for $T_{3,4}$ tetrahedra of 1.705 Å is lower than expected. Since we have assumed the framework disorder in the structure, this accounts for the difference in T–O for nominally 'Si' and 'Al' tetrahedra. In fact, our average $\langle$T–O$\rangle$ distance is in good agreement with the fully disordered eucryptite structure studied in [11]. The remaining difference may be caused by different cation coordination of the oxygen atoms and Li ordering in our structure. In beta-eucryptite the oxygen atoms are coordinated by one Si, one Al and one Li.

The O–O tetrahedral distances vary with temperature. The shortest value, 2.427 Å (figure 3) for the O_3–O_3 distance in the T_1 tetrahedron, and the longest, 2.798 Å for O_4–O_4 in the T_4 tetrahedron, are in good agreement with values in [16]. The mean angles $\langle$O–T–O$\rangle$ for all tetrahedra are almost identical and are 109.454° for $T_{3,4}$ tetrahedra and 109.593° for $T_{1,2}$

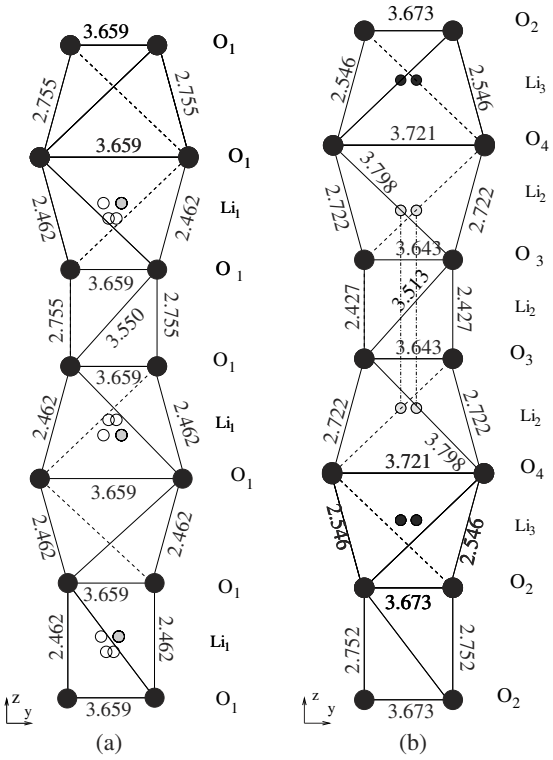

Figure 3. Structural channels in beta-eucryptite: (a) primary channel containing Li_1 atoms; (b) secondary channel containing Li_2 and Li_3. Li_2 is disordered over three tetrahedra. Li_1 and Li_2 atoms are represented by quartets, Li_3 atoms are represented by pairs. Quartets and pairs are arranged in a helical pattern in channels along the *c*-axis. O–O lengths are given in Å.

tetrahedra at 573 K (table 3), which is in good agreement with [11]. The mean $\langle O–T_{1,2}–O\rangle$ bond angles show an increase with temperature. However, the individual bond angles show a large spread (table 3). The Li ions cause nearby O–O distances for Si/Al tetrahedra to shorten, with a corresponding large spread of the tetrahedral angles [18]. In an ideal structure, all lithium coordination tetrahedra are in contact with T_1, T_2 and T_3 tetrahedra [11, 16]. Li coordination tetrahedra are not found adjacent to T_4 sites. In our structure disorder over all T sites changes the sizes of Li coordination tetrahedra. Consequently, the Li_2 ion, which is adjacent to the T_1 site, disorders over the originally vacant sites adjacent to the T_4 tetrahedron. This causes an increase in standard deviation of $\langle O–T_1–O\rangle$ and $\langle O–T_4–O\rangle$ (table 3). Furthermore, both of these standard deviations and hence angle variations rapidly increase with temperature. The angles around T_2 and T_3, in comparison to the angles around T_4, have smaller standard deviations and both ranges decrease with temperature.

Figure 4 shows the change in average $\langle T–O\rangle$ bond length versus temperature. The average T_4–O bond undergoes a change from 1.71 Å at 623 K to 1.68 Å at 743 K and changes slightly up to 873 K. The biggest change in $\langle T–O\rangle$ bond lengths happens before the phase transition at 758 K on heating. After the phase transition there is almost no change in bond lengths. The estimated temperature for this anomaly is 758 ± 5K. This T_c value is in good agreement with values from [9] and is in general agreement with the previously published transition temperatures ranging from 673 to 755 K [8, 19, 11]. Press *et al* [9] showed that there are two phase transitions around this temperature, at 755.5 ± 5 and 763 ± 5 K. The transition at 755.5 K is associated with condensation at the M-point of the Brillouin zone and causes a doubling of the cell in *a*. The second one, at 763 K, is the point of formation of the incommensurate phase, with Li modulated ordering in the structure. Our data show one transition at 758 ± 5 K,

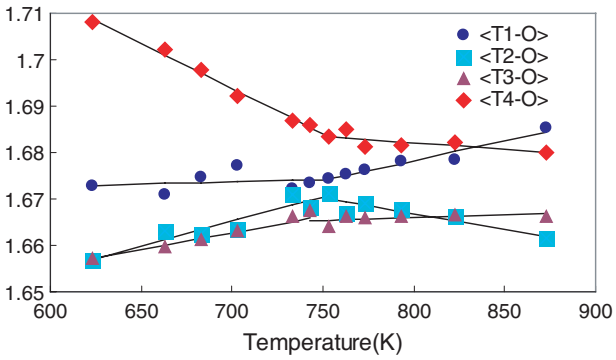

Figure 4. Average ⟨T–O⟩ bonds versus temperature for beta-eucryptite, with linear fits. $T_{1,2}$ are nominally 'Si' atoms, $T_{3,4}$ are nominally 'Al' atoms. The transition at 758 ± 5 K has a displacive character. Errors are smaller then the points.

(This figure is in colour only in the electronic version)

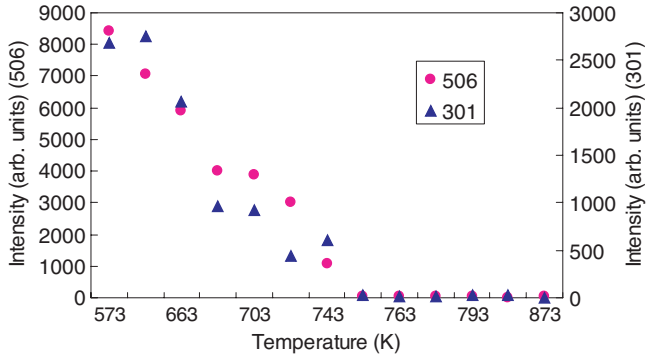

Figure 5. Intensities of peaks (301) and (506) versus temperature. Both peaks disappear around 758 K.

(This figure is in colour only in the electronic version)

which is in between these two temperatures. It is possible that we are observing processes connected to both the appearance of the modulated phase and doubling of the cell along the *a*-axis happening at the same point. To confirm this we have tried to observe a change in the intensities of peaks (*hkl*) with h = odd and which have larger contributions of lithium and oxygen atoms to their structure factors. We were able to observe the disappearance of peaks such as (301) or (506) around 758 K, which is associated with the doubling of the cell parameter in *a* (figure 5). Furthermore, the changes in mean ⟨T–O⟩ bond lengths and mean ⟨O–T–O⟩ bond angles suggest that the transition has a displacive character. The temperature resolution of our data does not allow us to determine the exact temperature for both of the processes, so further quantitative calculations would be speculative.

3.2. Li mobility and transition at 698 K

A single unit cell contains one primary channel and three secondary channels running parallel to [001]. In an idealized structure, i.e. without distortion in the Si/Al framework, the primary channel is small and the secondary channels are larger. Li_1 atoms are situated in the primary channel and are adjacent to T_3 (nominal 'Al') tetrahedra. Li_2 and Li_3 are both in the secondary channels and in the ideal model they occupy places within $T_{1,2}$ (nominal 'Si') layers.

Li occupies sites in the channels which are fourfold coordinated by oxygens. The ordered structure of Tscherry *et al* [16] requires that only half of the available Li sites be occupied. Occupied and vacant sites alternate along each framework channel parallel to the *c*-axis. However, Xu *et al* [11] showed that 20% of Li_1 atoms at room temperature are in the vacant sites and 80% are in ideal sites. Similarly for the secondary channel they found the ratio 95%:5%. Knowing that disorder occurs with increasing temperature, with Li atoms in channels diffusing

Table 4. Li–O distances in Å for beta-eucryptite at 573, 743 and 873 K. Four Li_1–O_1 distances are between four Li_1 quartets and O_1. Errors on all distances are smaller than 0.0001 Å.

	573 (K)	743 (K)	873 (K)		573 (K)	743 (K)	873 (K)
Li_1'–O_1	1.989	2.133	2.228	Li_1'''–O_1	1.825	2.112	2.017
Li_1''–O_1	2.314	2.604	2.718	Li_1''''–O_1	1.978	1.600	1.545
Mean $\langle Li_1'–O_1\rangle$	1.907	2.123	2.123	Mean $\langle Li_1''–O_1\rangle$	2.146	2.102	2.132
Li_2'–O_3	2.371	2.021	2.133	Li_2'–O_4	2.020	2.140	2.024
Li_2''–O_3	1.978	2.425	2.437	Li_2''–O_4	2.090	1.975	2.070
Mean $\langle Li_2–O_3\rangle$	2.183	2.223	2.285	Mean $\langle Li_2–O_4\rangle$	2.055	2.058	2.047
Li_3'–O_2	1.963	2.104	2.038	Li_3'–O_4	1.904	1.994	1.982
Li_3''–O_2	2.266	2.262	2.398	Li_3''–O_4	2.019	1.969	1.999
Mean $\langle Li_3–O_2\rangle$	2.114	2.183	2.218	Mean $\langle Li_3–O_4\rangle$	1.961	1.982	1.990

to the alternate sites, we explored the influence of Li positional disorder in the refinement. However, this did not improve the fit significantly ($R_{wp} = 11.33\%$) and the schemes we attempted proved to be unstable. Refinement for all data sets was completed using only the occupied Li sites. Instead we used a split Li model, which showed that only Li_2 ions diffuse into the vacant site, but Li_1 and Li_3 ions remain close to their ideal sites (figure 3). This explains why the model of Xu *et al* [11] did not fit our dataset successfully.

As we used the split-atom model to fit the disorder of Li ions, we have four partial bonds in each LiO_4 tetrahedron, with four distances between O and Li quartets and pairs (figure 3).

The mean $\langle Li_1'–O_1\rangle$ distance of 1.907 Å (table 4) is the shortest distance of all the mean values found in Li coordination tetrahedra. It is shorter than the corresponding value of 1.99 Å from [16]. The shared edge with the T_3 tetrahedra, for example, O_1–O_1 is equal to 2.462 Å (figure 3). This is the shortest edge for both T_3 (nominally 'Al_1') and Li_1 coordination tetrahedra. The longest intertetrahedral[3] O_1–O_1 distance for Li_1 coordination tetrahedra is 3.55 Å (figure 3). The large difference between these two distances show the deviation of Li coordination tetrahedra from a regular tetrahedron. The difference between $\langle Li_1'–O_1\rangle$ and $\langle Li_1''–O_1\rangle$ decreases with temperature; their ratio changes from 0.88 at 573 K to almost 1 at 873 K.

Both the $\langle Li_2–O_3\rangle$ and $\langle Li_2–O_4\rangle$ distances, 2.183 and 2.055 Å, are larger than the expected 1.98 Å [16]. The intratetrahedral distance O_3–O_3 is only 2.427 Å, which is a short distance for adjacent T_1 (nominally 'Si_1') tetrahedra. For comparison Tscherry *et al* quote 2.48 Å for the corresponding bond as being very short [16]. The largest O_3–O_3 intertetrahedral distance for Li_2 coordination tetrahedra is 3.513 Å, which is the shortest intertetrahedral O–O distance (figure 3).

The ratio D between largest and smallest O–O distances in all three tetrahedra is 1.44 for the Li_1 tetrahedron, 1.49 for the Li_2 tetrahedron and 1.44 for the Li_3 tetrahedron. The large difference for the Li_2 tetrahedron reflects the distortion of the site and explains why Li_2 ions are disordered over the two neighbouring tetrahedra (for which $D = 1.39$)—due to repulsion between O and Li ions (figure 3).

Since we used the split-atom model to describe the behaviour of Li atoms, we can use the magnitudes of the splitting to describe the transition. Press *et al* [9] showed that this is a transition between commensurate and incommensurate structures, with Li modulation in the

[3] The O–O distances which are shared between Li coordination tetrahedron and Si/Al tetrahedra are called here intratetrahedral bonds, for example, O_3–$O_3 = 2.4$ Å in Li_2 coordination tetrahedron. The longest O–O bond distances in Li coordination tetrahedra, like O_3–$O_3 = 3.5$ Å in Li_2 coordination tetrahedron, are called intertetrahedral bonds (figure 3).

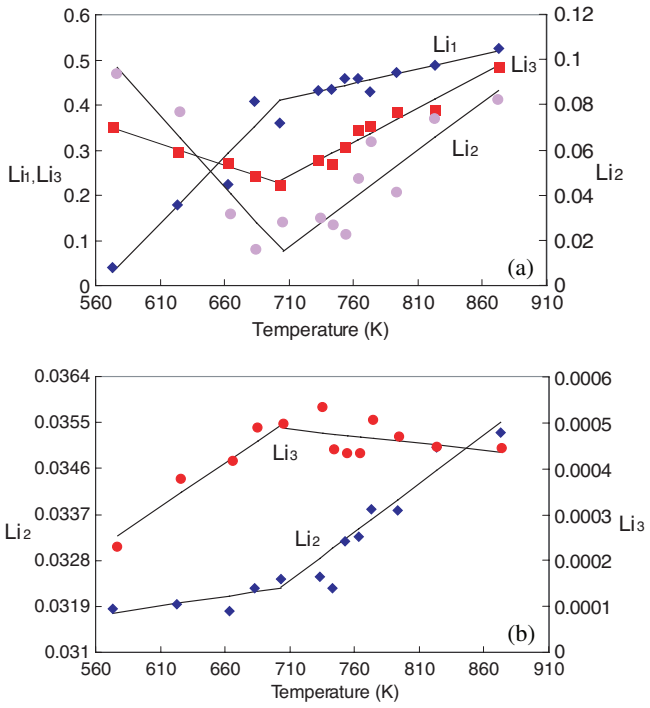

Figure 6. (a) Deviation of Li_1, Li_2 and Li_3 atoms from their ideal positions in the xy-plane versus temperature. (b) Deviation of Li_2 and Li_3 atoms from their ideal positions in the z-plane versus temperature.

(This figure is in colour only in the electronic version)

structural channels. The deviation of pairs and quartets of the Li atoms from their ideal position in the xy-plane, V_{xy}, and in the z-direction, V_z, can give us a good estimate of this transition:

$$V_{xy}^2 = [(\Delta x - \tfrac{1}{2}\Delta y)^2 + (\tfrac{3}{4})\Delta y^2]a^2 \tag{1}$$

$$V_z^2 = \Delta z^2, \tag{2}$$

where a is a cell parameter; Δx, Δy and Δz are deviations from high symmetry sites. This is true because the deviation in the xy-plane is equal to

$$V_{xy} = \Delta x\vec{a} + \Delta y\vec{b} = \left(\Delta x - \frac{\Delta y}{2}, \frac{\Delta y\sqrt{3}}{2}, 0\right)a. \tag{3}$$

The deviations of all Li atoms in the xy-plane and in the z-direction change around 698 K (figure 6). For Li_1 it climbs from 0.04 at 573 K to 0.42 at 698 K and then slowly increases up to 0.53 at 873 K. In contrast, for Li_2 and Li_3, the deviation decreases from 573 up to 698 K. We see a big change from 0.35 to 0.22 for Li_3 and a considerably smaller change for Li_2 from 0.09 to 0.015 in the same temperature range. After the phase transition, at 698 K, the smallest change happens with Li_2 from 0.015 to 0.082 at 873 K. For Li_1 the change is from 0.42 up to 0.52 at 873 K and finally the biggest changes are with Li_3 from 0.22 at 698 K to 0.48 at the highest temperature. A large deviation of Li atoms in the xy-plane corresponds to the vibration inside the Li coordination tetrahedron. Above the Li order–disorder phase transition at 685 K, all three atoms show increases in their positional disorder, inside the Li coordination tetrahedron. Note that deviations for Li_2 and Li_3, which are present in the secondary channels, show similar variations. Li_1, found in the primary channel, undergoes different changes.

Li disorder shortens the O–O bond distances for Si/Al tetrahedra, which means that changes in O_3–O_3 bond length and O_3–T_1–O_3 bond angle are connected to the disorder in the Li_2 ions over the three tetrahedra (figure 3). Li_2 coordination tetrahedra share the O_3–O_3

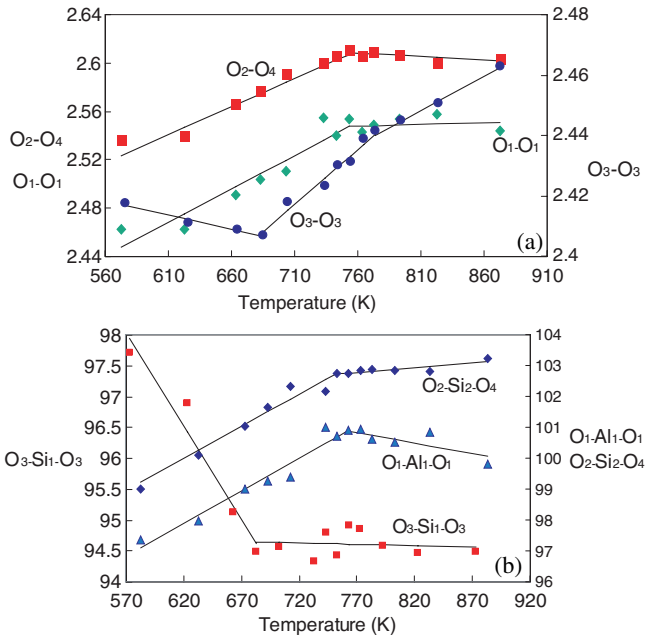

Figure 7. (a) O_3–O_3, O_1–O_1 and O_2–O_4 bond distances in Å versus temperature. Note that O_3–O_3 is the smallest among these three bond lengths; (b) O_3–T_1–O_3, O_2–T_2–O_4 and O_1–T_3–O_3 bond angles in degrees versus temperature. Note that O_3–T_1–O_3 is the smallest angle amongst the three others.

(This figure is in colour only in the electronic version)

edge with T_2 tetrahedra. The corresponding value for the O_3–O_3 distance here is 2.427 Å at 573 K, decreasing with temperature until approximately 698 K (figure 7). Furthermore, on heating, there is a sharp rise with a small change of slope around 785 K. The O_3–T_1–O_3 bond angle decreases with temperature until 698 K. These dramatic changes for O_3–O_3 distance and O_3–T_1–O_3 bond angle show the Li_2 disorder. By contrast, O_1–O_1 and O_2–O_4 distances and O_1–T_3–O_3 and O_2–T_2–O_4 bond angles are not affected by the Li order–disorder transition at 698 K, but instead by the framework distortion. Li_1 coordination tetrahedra share edges with T_3 tetrahedra and Li_3—with T_2 tetrahedra.

After the refinement, we used the GSAS internal program VRSTPLOT [14] to generate VRML files, which give the difference Fourier maps for Li ion motion at different temperatures. Figure 8 represents stereo-pairs of one unit cell of beta-eucryptite. The primary channels with Li_1 are at the corners of the unit cell. As one can see, the Li motion happens along the channels. Even at the highest temperatures, there is almost no cross-channel diffusion.

4. Conclusions

We have shown that some of the Li atoms are disordered over the ideal sites, as well as the vacant sites, compared to the ideal eucryptite structure. This was achieved by using a Li split-atom model to fit our data. For some structures there is no difference between fitting the model with split-atoms or a model with anisotropic temperature factors [20]. In the case of beta-eucryptite, fitting Li with anisotropic temperature factors proved to be very unstable, which was consistent with [12, 7]. The split Li atom model proved to give a better picture of the Li motion in the channels, allowing us to identify the disorder in L_2 over three adjacent tetrahedra and the motion of Li atoms in the xy-plane and the z-direction. Ultimately, the difference Fourier maps provide the best indication of Li ion disorder within the structure.

On cooling, beta-eucryptite undergoes a zone boundary transition at the M-point at 698 K. This is due to Li order–disorder in the structural channels with the appearance of the

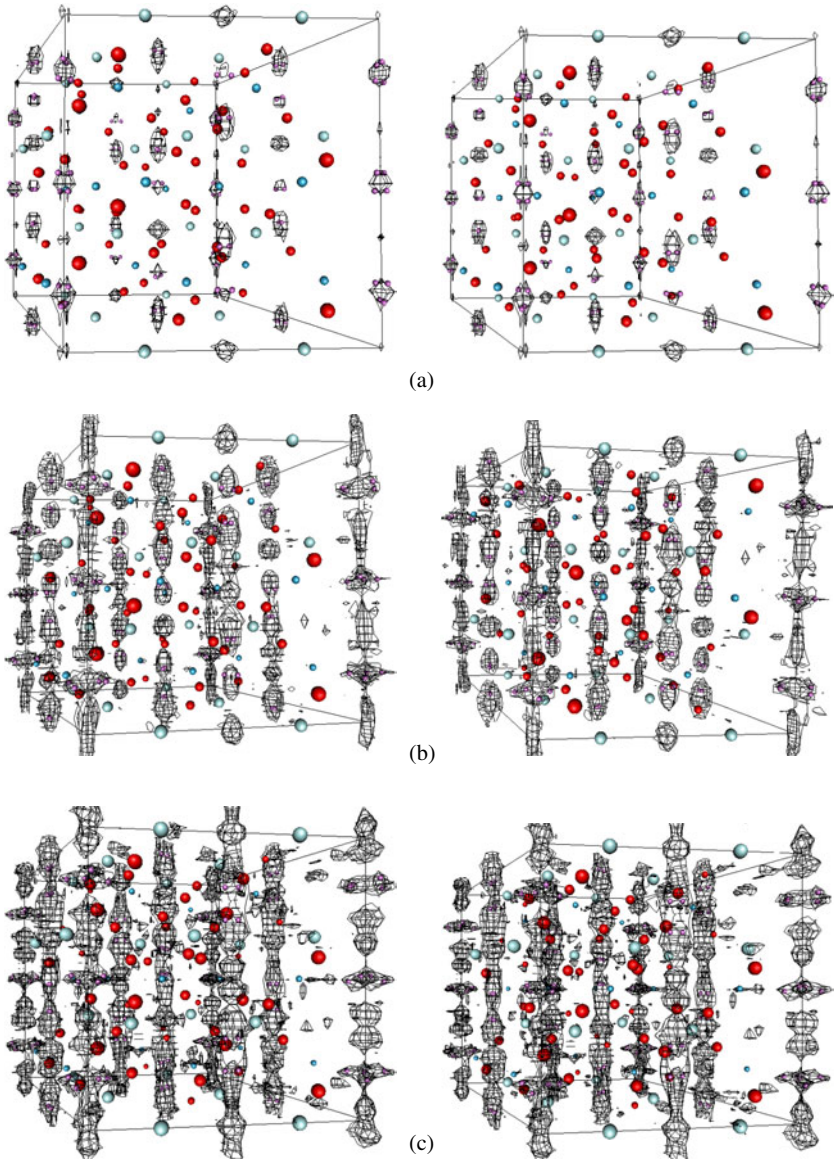

Figure 8. Stereo pairs of the difference Fourier map in 3D of one unit cell of beta-eucryptite. Dark (red) balls are oxygen atoms. Light balls (pale blue)—T_1, T_2, T_3 and T_4 (Si and Al). Li atoms are magenta in the online version. The contour lines represent the nuclear density corresponding to Li ion. (a) $T = 573$ K; (b) $T = 743$ K; (c) $T = 873$ K.

(This figure is in colour only in the electronic version)

commensurate structure. Although the cell parameters do not show changes at this temperature, parameters such as bond lengths and bond angles change dramatically. The deviation of the Li quartets and pairs from their ideal sites is affected by this transition significantly. The increase in lithium motion in the channels can be seen from the Fourier maps. There is no cross-motion between the channels up to 875 K (figure 8), and the material acts as a one-dimensional superionic conductor.

The Si/Al framework undergoes a displacive phase transition at the M-point at 758 K, on cooling, which is accompanied by the ordering of Li atoms and formation of the incommensurate structure. Above this transition point Li atoms disorder and channels become equivalent. These changes result in a halving of the *a* cell parameter. The bond lengths, bond angles and corresponding O–O bond lengths show interlinked changes at this phase transition. The large range of the previous reported T_c values is most likely due not only to different synthesis conditions of the samples but also probably to variations in the resolution of the analytical techniques used.

Acknowledgments

We would like to thank ILL for funding the experiment, Dr Alan Hewat for help with the experiment, and two anonymous reviewers for useful comments. AS thanks ICI for funding and S A Wells and A Walkingshaw for proofreading.

References

[1] Buerger M J 1954 The stuffed derivatives of silica structure *Am. Mineral.* **39** 600–14
[2] Nagel W and Bohm H 1982 Ionic conductivity in $LiAlSi_4$–SiO_2 solid solutions of the high quartz type *Solid State Commun.* **42** 625–31
[3] Hummel F A 1951 Thermal expansion properties of some synthetic lithio minerals *J. Am. Ceram. Soc.* **34** 235–9
[4] Lichtenstein A I, Jones R O, Xu H and Heaney P J 1998 Anisotropic thermal expansion in the silicate β-eucryptite: a neutron diffraction and density functional study *Phys. Status Solidi* **31** 723–37
[5] Schulz H 1974 Thermal expansion of beta-eucryptite *J. Am. Ceram. Soc.* **57** 313–7
[6] Winkler H G F 1948 Synthese und kristallstruktur des eukryptits, $LiAlSiO_4$ *Acta Crystallogr.* **1** 27–34
[7] Xu H, Heaney P J and Bohm H 1999 Structural modulations and phase transitions in β-eucryptite: an *in situ* TEM study *Phys. Chem. Minerals* **26** 633–43
[8] Pillars W P and Peacor D R 1973 The crystal structure of beta-eucryptite as a function of temperature *Am. Mineral.* **58** 681–90
[9] Press W, Renker B, Schulz H and Bohm H 1980 Neutron scattering of the one-dimensional ionic conductor β-eucryptite *Phys. Rev.* B **21** 1250–7
[10] Nara S, Yoshimitsu K and Matsubara T 1981 Phenomenological theory of phase transitions in β-eucryptite *Prog. Theor. Phys.* **66** 1143–59
[11] Xu H, Heaney P J and Yates D M 1999 Structural mechanisms underlying near-zero thermal expansion in β-eucryptite: a combined synchrotron x-ray and neutron Rietveld analysis *J. Mater. Resour.* **14** 3138–51
[12] Hornyak E J 1969 The crystal structure of $LiAlSiO_4$ and an electron spin resonance study of ferric iron in $LiAlSiO_4$ *PhD Thesis* University of Michigan, USA
[13] Zhang M, Xu H, Salje E K H and Heaney P J 2003 Vibrational spectroscopy of beta-eucryptite ($LiAlSiO_4$): optical phonons and phase transition(s) *Phys. Chem. Minerals* **30** 457–62
[14] Larson A C and Von Dreele R B 1994 General structure analysis system (GSAS) *Los Alamos National Laboratory Report* N LAUR 86–748 p 179
[15] Redfern S A T 2000 Order–disorder phase transitions *Transformation Processes in Minerals. Review in Mineralogy 39* ed S A T Redfern and M A Carpenter (Washington, DC: Mineralogical Society of America)
[16] Tscherry V, Schulz H and Laves F 1972 Average and super structure of β-eucryptite ($LiAlSiO_4$), part II: super structure *Z. Kristallogr.* **135** 175–98
[17] Jones J B 1968 Al–O and Si–O distances in aluminosilicate framework structures *Acta Crystallogr.* B **14** 355–8
[18] Palmer D C 1994 Stuffed derivatives of silica polymorphs *Silica. Reviews in Mineralogy 29* ed P J Heaney, C T Prewitt and G V Gibbs (Washington, DC: Mineralogical Society of America)
[19] Tscherry V and Laves F 1970 Synthesis and x-ray reflection pattern of β-eucryptite ($LiAlSiO_4$) *Naturwissenschaften* **57** 194
[20] Megaw H D 1969 Comparison of effects of temperature factor and 'splitting of atoms' *Acta Crystallogr.* B **25** 1516–8